

From traffic and pedestrian follow-the-leader models with reaction time to first order convection-diffusion flow models

Antoine Tordeux* Guillaume Costeseque† Michael Herty‡ Armin Seyfried§

December 14, 2016

Abstract

In this work, we derive first order continuum traffic flow models from a microscopic delayed follow-the-leader model. Those are applicable in the context of vehicular traffic flow as well as pedestrian traffic flow. The microscopic model is based on an *optimal* velocity function and a reaction time parameter. The corresponding macroscopic formulations in Eulerian or Lagrangian coordinates result in first order convection-diffusion equations. More precisely, the convection is described by the optimal velocity while the diffusion term depends on the reaction time. A linear stability analysis for homogeneous solutions of both continuous and discrete models are provided. The conditions match the ones of the car-following model for specific values of the space discretization. The behavior of the novel model is illustrated thanks to numerical simulations. Transitions to collision-free self-sustained stop-and-go dynamics are obtained if the reaction time is sufficiently large. The results show that the dynamics of the microscopic model can be well captured by the macroscopic equations. For non-zero reaction times we observe a scattered fundamental diagram. The scattering width is compared to real pedestrian and road traffic data.

Keywords: First order traffic flow models, micro/macro connection, hyperbolic conservation laws, Godunov scheme, numerical simulation.

AMS: 35F20, 70F45, 90B20, 65M12.

1 Introduction

Microscopic and macroscopic approaches for the purpose of vehicular traffic flow modelling have been often developed separately in the engineering community [43, 22, 5, 25]. Similar models can also be used in the description of pedestrian dynamics [40, 10, 1]. Typically, microscopic models are based on the so-called “follow-the-leader” strategy and they are stated as (finite or infinite) systems of Ordinary Differential Equations (ODEs). They are generally based on speed or acceleration functions which depend on distance spacing, speed, predecessor’ speed, relative speed and so on. One of the simplest approach is a speed model solely based on the spacing, firstly proposed by Pipes [38]

$$\dot{x}_i(t) = W(\Delta x_i(t)), \quad (1)$$

where $\Delta x_i(t) = x_{i+1}(t) - x_i(t)$ denotes the spacing between the vehicle (i) to its predecessor ($i + 1$) and $W(\cdot)$ stands for the equilibrium (or optimal) speed function depending on the spacing. The microscopic models are discrete in the sense that the vehicles or pedestrians $i \in \mathbb{Z}$ are

*Forschungszentrum Jülich GmbH and Bergische Universität Wuppertal, Germany (a.tordeux@fz-juelich.de).

†INRIA Sophia Antipolis-Méditerranée, France (guillaume.costeseque@inria.fr).

‡Rheinisch-Westfälische Technische Hochschule Aachen, Germany (herty@igpm.rwth-aachen.de).

§Forschungszentrum Jülich GmbH and Bergische Universität Wuppertal, Germany (a.seyfried@fz-juelich.de).

individually considered. A macroscopic description consider the flow of vehicles or pedestrians (in the following also referred to as *agents*) as a continuum in Eulerian or Lagrangian coordinates. For instance in the most classical Eulerian time-space framework, the main variables are the density, the flow and the mean speed. The simplest approach is the scalar hyperbolic equation of the celebrated Lighthill-Whitham-Richards (LWR) model [29, 39]

$$\partial_t \rho + \partial_x(\rho V(\rho)) = 0. \quad (2)$$

Here ρ is the density, $V(\cdot)$ is the equilibrium speed function which is assumed to depend only on the density. The flow $f(\rho) = \rho V(\rho)$ is given by the product of the density times the mean speed. The model is derived from the continuity equation for which the flow is supposed in equilibrium. The microscopic and macroscopic models Eq. (1) and Eq. (2) well reproduce shock-wave phenomena for Riemann problems. Yet such models are not able to describe the observed transition to scattered flow/density relation (the fundamental diagram) with hysteresis and self-sustained stop-and-go phenomena (see [44, 24, 9] and Fig. 1). This is due to the fact that spatially homogeneous regime are always in the equilibrium solutions and determined by the functions $W(\cdot)$ and $V(\cdot)$, respectively.

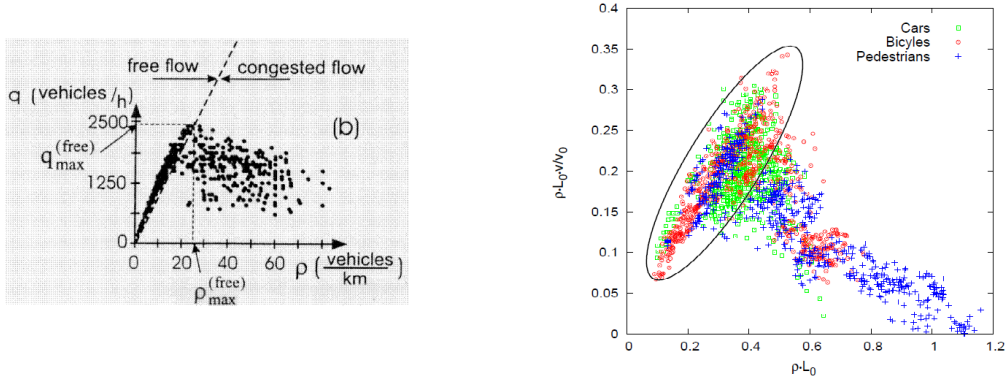


Figure 1: Empirical fundamental diagrams. Left, [23, Figure 1] and right, [48, Figure 5].

Therefore, the microscopic behavior is modified by introducing reaction and relaxation times. The simplest following model of this type may be the delayed model by Newell [31]

$$\dot{x}_i(t + \tau) = W(\Delta x_i(t)), \quad (3)$$

with τ the reaction time (if positive). Applying a Taylor expansion in the l.h.s. of the delayed speed model Eq. (3), we obtain the second order ‘optimal velocity model’ (OVM) introduced by Bando *et al.* in [4]. The OVM has limit-cycles in stationary states, with self-sustained propagation of non-linear stop-and-go waves, and hysteresis curves in the fundamental flow/density diagram (see [34, 35]). Macroscopic second-order models comprised of systems of hyperbolic equations are also able to reproduce non-linear stop-and-go waves and scattering of the fundamental diagram. One of the first approach is the one by Payne and Whitham [37, 46]. The model can be derived from the microscopic Newell model Eq. (3). The main drawback of this model is that, as pointed out by Daganzo [13], the speed and the density could yield negative values and are not bounded. Note that this drawback is also observed with follow-the-leader models like the OVM and is referred as collision between the vehicles (see for instance [14, 36] or [43, Chap. 15]). Aw and Rascle have corrected this issue by replacing the space derivative

of the ‘pressure’ by a convective derivative [3] (AR model). Nowadays extensions of the AR model such as the ARZ, GARZ or generalized models [21, 47, 6, 17, 41, 16], as well as two phase models coupled with the LWR model [11, 19, 12, 7], are used to describe transition to congested traffic with scattered fundamental diagrams and self-sustained non-linear shock waves. A general framework is the generic second order model (GSOM) family introduced in [27, 28]. Most of the approaches are a posteriori based on the continuous description.

In this article, we derive minimalist macroscopic traffic flow models of first order from a microscopic speed model to describe stop-and-go wave phenomena and scattering of the fundamental diagram. The use of first order models allow us to ensure by construction that the speed and the density remain positive and bounded. The starting point is a OV microscopic model of first order including a reaction time parameter. We show in Sec. 2 that the corresponding macroscopic model results in a convection-diffusion equation. The macroscopic model is discretized using distinct Godunov and Euler-based schemes and the linear stability conditions for the homogeneous solutions of these numerical schemes are provided in Sec. 3. The conditions match the ones of the car-following model for specific values of the spatial discretization step. Simulations are carried out in Sec. 4. Systems with different initial conditions are numerically solved. Further, we compare with data of realistic traffic flow as well as pedestrian flow.

2 Microscopic and macroscopic models

2.1 The microscopic follow-the-leader model

The microscopic model we use has been introduced in [42]. It is based on the Newell model Eq. (3). In the remaining of the paper, we assume that $W : s \mapsto W(s)$ is Lipschitz continuous, non-decreasing and upper bounded in order to get the well-posedness of Eq. (3) supplemented with initial conditions $x_i(t = 0) = x_{i,0}$ for any $i \in \mathbb{Z}$. We rewrite the equation as

$$\dot{x}_i(t) = W(x_{i+1}(t - \tau) - x_i(t - \tau)), \quad (4)$$

and apply a Taylor expansion in the argument of W . Neglecting higher-order terms in τ we obtain

$$\dot{x}_i(t) = W(\Delta x_i(t) - \tau[W(\Delta x_{i+1}(t)) - W(\Delta x_i(t))]). \quad (5)$$

The model is a system of ordinary differential equations of first order with two predecessors in interaction. It is calibrated by the delayed time $\tau \in \mathbb{R}$, that is a reaction time if positive and an anticipation time if negative, and the optimal speed function $W(\cdot)$. The function $W(\cdot)$ is supposed to be bounded by $V_0 > 0$, positive and zero if the spacing is smaller than ℓ , $\ell > 0$ being the vehicle’s length or size of the pedestrian. Note that the model admits a minimum principle, say $\Delta x_i(t) \geq \ell \forall i, t$. Thus it is by construction collision-free and it has the same stability condition as the initial microscopic Newell model Eq. (3) or as the OVM from [4]. This condition is for all $s \in \mathbb{R}$

$$|\tau|W'(s) < 1/2. \quad (6)$$

Note that the condition simply reduces to $|\tau| < T/2$ if one considers the linear fundamental diagram $W : s \mapsto W(s) := \max\{0, \min\{\frac{1}{T}(s - \ell), V_0\}\}$, with $T > 0$. When unstable, the model transits to states with collision-free self-sustained stop-and-go dynamics, see [42].

2.2 Derivation of macroscopic models

In the following, we consider $i = 1, \dots, N$ agents with periodic boundary conditions (i.e. the predecessor of the agent N is the agent 1). The derivation of macroscopic models from microscopic

models is useful to fully understand the dynamics. In [2], Aw *et al.* established the connection between a microscopic car-following model and the second-order AR macroscopic traffic flow model. The rigorous proof, based on a scaling limit where the time and space linearly increase while the speed and the density remain constant, assumes homogeneous conditions. We use here the same methodology considering the local density $\rho_i(t)$ around the vehicle or pedestrian (i) and at time $t > 0$, as the inverse of the spacing

$$\rho_i(t) := \frac{1}{\Delta x_i(t)}. \quad (7)$$

The density could also be normalized by multiplication with ℓ . Here, we prefer to keep the unit of one over length as density to ease the comparison with the classical models. Then, the microscopic model reads

$$\dot{x}_i(t) = W \left(\frac{1}{\rho_i(t)} - \tau \left[W \left(\frac{1}{\rho_{i+1}(t)} \right) - W \left(\frac{1}{\rho_i(t)} \right) \right] \right) =: \tilde{V}(\rho_{i+1}(t), \rho_i(t)), \quad (8)$$

for a velocity profile \tilde{V} . Then,

$$\partial_t \frac{1}{\rho_i(t)} = \partial_t \Delta x_i(t) = \tilde{V}(\rho_{i+2}(t), \rho_{i+1}(t)) - \tilde{V}(\rho_{i+1}(t), \rho_i(t)). \quad (9)$$

In [2] it has been observed that Eq. (9) is a semi-discretized version of hyperbolic partial differential equation in Lagrangian coordinates. This requires to consider limits of many vehicles or pedestrians $N \rightarrow \infty$ and diminishing length $\ell \rightarrow 0$. We introduce the continuous variable $y \in \mathbb{R}$ such that $y_i = i\Delta y$ as counting variable for the number of agents where Δy is proportional to ℓ . By piecewise constant extension of the given spacing, we construct a density $\rho(t, y)$ such that $\frac{1}{\rho_i(t)} = \frac{1}{\Delta y} \int_{y_i - \frac{\Delta y}{2}}^{y_i + \frac{\Delta y}{2}} \frac{1}{\rho(t, z)} dz$. The quantity $\frac{1}{\rho_i(t)}$ is the volume average over a cell of length Δy centered at y_i . The r.h.s. of (9) describes the flux across the cell boundaries. Introduce $V : k \mapsto V(k) = W\left(\frac{1}{k}\right)$ for any $k > 0$. Then, it follows that $\tilde{V}(k_1, k_2) = V\left(\frac{k_2}{1 - k_2\tau[V(k_1) - V(k_2)]}\right)$ for any $(k_1, k_2) \in (0, +\infty)^2$ satisfying $V(k_1) \neq V(k_2) + \frac{1}{\tau k_2}$. As for OVM, W is non-decreasing, therefore we observe that V is non-increasing on $(0, +\infty)$. We obtain from (9)

$$\partial_t \frac{1}{\rho_i(t)} - \frac{\Delta y}{\Delta y} \left[V \left(\frac{\rho_{i+1}}{1 - \tau \rho_{i+1} Z_{i+1}} \right) - V \left(\frac{\rho_i}{1 - \tau \rho_i Z_i} \right) \right] = 0, \quad (10)$$

where $Z_i := V(\rho_{i+1}) - V(\rho_i)$. Provided that $-V$ is increasing and $\rho(t, y)$ is piecewise constant on each cell, the reconstruction at the cell interface $y_{i \pm \frac{1}{2}}$ is given by cell averages, i.e., $\frac{1}{\rho\left(t, y_{i \pm \frac{1}{2}}\right)} = \frac{1}{\rho_{i+1}(t)}$. Next, we rescale time $t \rightarrow t\Delta y$ and also reaction time $\tau \rightarrow \tau\Delta y$ to obtain

$$\partial_t \frac{1}{\rho_i(t)} - \frac{1}{\Delta y} \left[V \left(\frac{\rho_{i+1}}{1 - \tau \rho_{i+1} \frac{Z_{i+1}}{\Delta y}} \right) - V \left(\frac{\rho_i}{1 - \tau \rho_i \frac{Z_i}{\Delta y}} \right) \right] = 0. \quad (11)$$

Hence, we observe that in the rescaled time and in the limit $\Delta y \rightarrow 0$ the microscopic model is an upwind discretization of the following macroscopic equation

$$\partial_t \frac{1}{\rho} - \partial_y V \left(\frac{\rho}{1 - \tau \rho \partial_y V(\rho)} \right) = 0. \quad (12)$$

The upwind or Godunov scheme is the most mathematically reasonable discretization provided τ is sufficiently small due to the decreasing behavior of V for suitable OVM functions W . Up to

second-order in τ we approximate (12) by Taylor expansion and obtain a convection–diffusion model as

$$\partial_t \frac{1}{\rho} - \partial_y V(\rho) = \tau \partial_y ((\rho V'(\rho))^2 \partial_y \rho). \quad (13)$$

The relation between the density in Lagrangian coordinates and Eulerian coordinates is given by the coordinate transformation $(t, y) \rightarrow (t, x)$ where $y = \int_{-\infty}^x \rho(t, x) dx$. Note that y counts the number of vehicles/pedestrians up to position x in Eulerian coordinates. In the Eulerian coordinates (t, x) , the macroscopic model Eq. (12) reads

$$\partial_t \rho + \partial_x \left(\rho V \left(\frac{\rho}{1 - \tau \partial_x V(\rho)} \right) \right) = 0. \quad (14)$$

The model could be seen as an extension of the LWR model Eq. (2) with a modified speed-density relationship $\rho \mapsto V(\rho/(1 - \tau \partial_x V(\rho)))$. For illustrating the behavior of this modified speed-density mapping, we set $I := \tau \partial_x V(\rho)$ and we define $\mathcal{V} : (\rho, I) \mapsto V(\rho/(1 - I))$. The fundamental diagrams obtained for a constant term $I \in \{-0.3, 0, 0.3\}$ and for a speed function $V : \rho \mapsto \max\{0, \min\{2, 1/\rho - 1\}\}$ are shown on Figure 2. Note that for constant (in space) densities ρ (and/or for $\tau = 0$), the additional term I vanishes and we recover the classical LWR model.

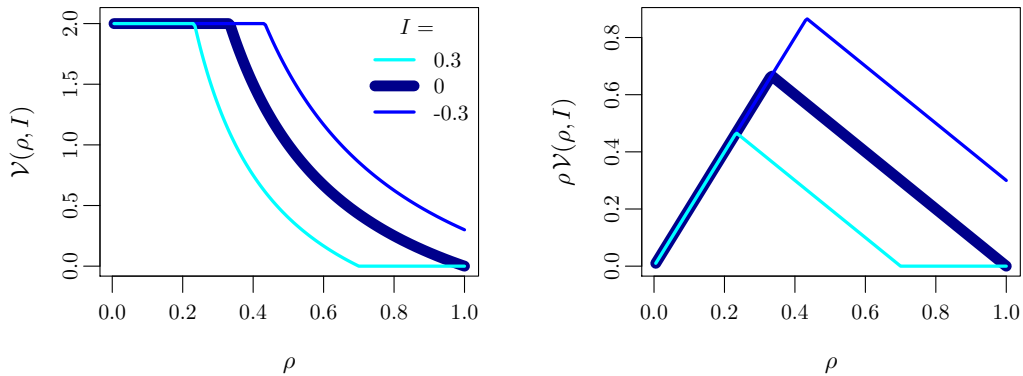


Figure 2: Illustration for the fundamental diagram $\mathcal{V} : (\rho, I) \mapsto V(\rho/(1 - I))$ obtained in the macroscopic model (14) with constant inhomogeneity $I \in \{-0.3, 0, 0.3\}$ and $V : \rho \mapsto \max\{0, \min\{2, 1/\rho - 1\}\}$.

3 Linear stability analysis

3.1 Linear stability analysis of the continuous macroscopic model

A Taylor expansion up to second-order in terms of τ for equation (14) yields

$$\partial_t \rho + \partial_x (\rho V(\rho)) = -\tau \partial_x ((\rho V'(\rho))^2 \partial_x \rho). \quad (15)$$

We also consider an initial condition

$$\rho(t = 0, x) = \rho_0(x) \quad \text{for any } x \in \mathbb{R} \quad (16)$$

where $\rho_0 \in L^1(\mathbb{R}) \cap \text{BV}(\mathbb{R})$. By defining $D(\rho) := \int_{-\infty}^x -\tau(\rho V'(\rho))^2 \partial_x \rho \, dy$, we obtain an equation similar to the one considered in [8], say

$$\partial_t \rho + \partial_x(\rho V(\rho)) = \partial_x^2 D(\rho). \quad (17)$$

One can verify that $D(\rho_0)$ is absolutely continuous on \mathbb{R} and that $\partial_x D(\rho_0) \in \text{BV}(\mathbb{R})$. In (15), the l.h.s. is the LWR model with additional diffusion proportional to the reaction time parameter τ and that can be either negative or positive. More precisely the diffusion is negative in deceleration phases where the density get higher upstream, and it is positive in the opposite acceleration phases. This type of diffusion seems to induce an instability of the homogeneous (constant) solutions and the formation of oscillations (i.e. jam waves). The diffusion coefficient $(\rho V'(\rho))^2$ depends on the density and the fundamental diagram. In fluid dynamics the coefficient is a characteristic for the flexibility of the random movement responsible for the diffusion. In traffic flows, comparable diffusion-convection forms have been used in [30, 8]. We refer the interested reader to [8] (and references therein) for a proof of existence and uniqueness of the solution to Eq. (15)-(16). In the following we analyze the linear stability of homogeneous solutions for the macroscopic model.

Proposition 3.1 *The homogeneous configurations for which $\rho(x, t) = \rho_e$ for all x and t are linearly stable for the continuous traffic model Eq. (15) if and only if*

$$\tau < 0. \quad (18)$$

Note that a negative τ refers to an anticipation time.

Proof If $\varepsilon(x, t) = \rho(x, t) - \rho_e$ is a perturbation to homogeneous solution ρ_e , then

$$\varepsilon_t = F(\rho_e + \varepsilon, \varepsilon_x, \varepsilon_{xx}) = \alpha \varepsilon + \beta \varepsilon_x + \gamma \varepsilon_{xx} + o(LC(\varepsilon, \varepsilon_x, \varepsilon_{xx})), \quad (19)$$

with $F(\rho, \rho_x, \rho_{xx}) = -\partial_x(\rho V(\rho) - \tau(\rho V'(\rho))^2 \partial_x \rho)$, $\alpha = \frac{\partial F}{\partial \rho}(\rho_e, \rho_e, \rho_e) = 0$, $\beta = \frac{\partial F}{\partial \rho_x}(\rho_e, \rho_e, \rho_e) = -V(\rho_e) - \rho_e V'(\rho_e)$, $\gamma = \frac{\partial F}{\partial \rho_{xx}}(\rho_e, \rho_e, \rho_e) = -\tau(\rho_e V'(\rho_e))^2$. The solutions of the linear system are the Ansatz $\varepsilon = z e^{\lambda t - i x l}$ where $\lambda \in \mathbb{C}$, $x, l \in \mathbb{R}$. We get $\varepsilon_t = \lambda \varepsilon$, $\varepsilon_x = -i l \varepsilon$ and $\varepsilon_{xx} = -l^2 \varepsilon$. Therefore the characteristic equation of the perturbed system Eq. (19) is $\lambda_l = \tau(l \rho_e V'(\rho_e))^2 + i l (V(\rho_e) + \rho_e V'(\rho_e))$. The homogeneous solution are stable when $\varepsilon \rightarrow 0$, i.e. $\Re(\lambda_l) < 0$ for all $l > 0$. This holds only if the diffusion is positive. This is $\tau < 0$. ■

Therefore the macroscopic model is unstable as soon as the reaction time τ is positive which is the physically reasonable case. An explanation is that the Taylor expansion of the original model in terms of τ does lead to a perturbed equation with different properties. However, the discrete model does not have this stability requirement. Therefore, we show below that for suitable discretization of the model we recover stability. □

3.2 Linear stability analysis for the discrete schemes

Discretizations of the macroscopic models Eqs. (12) and (13) in ‘Lagrangian’ coordinates give the initial microscopic model Eq. (5). Our purpose in this section is the discretization of the macroscopic models Eqs. (14) and (15) in Eulerian coordinates. We denote dt and dx the time

and spatial discretization steps and use the Godunov scheme [20] for the discretization of the density

$$\rho_i(t + dt) = \rho_i(t) + \frac{dt}{dx}(f_{i-1}(t) - f_i(t)) \quad (20)$$

where f_i denotes the flow at cell boundary and has to be determined. For this aim, we introduce the *demand* and *supply* functions from the flow-density fundamental diagram $f : \rho \mapsto f(\rho) := \rho V(\rho)$ as first proposed in [13, 26] and that read respectively

$$\Delta(\rho) := \max_{k \leq \rho} f(k) \quad \text{and} \quad \Sigma(\rho) := \max_{k \geq \rho} f(k) \quad (21)$$

and we define the Godunov flux as $G(x, y) := \min\{\Delta(x), \Sigma(y)\}$. We are now ready to propose three different strategies to compute the boundary flows f_i . The first two methods discretize the linearized model Eq. (15) using a splitting scheme which treats separately the convection and the diffusion terms. The last scheme is a simple discretization of the exact macroscopic model Eq. (14).

1. **The Godunov/Euler scheme:** a Godunov scheme for the convection term and an explicit Euler scheme for the diffusive term of the linearised model Eq. (15):

$$f_i^{(1)} = G(\rho_i, \rho_{i+1}) + \frac{\tau}{dx}(\rho_i V'(\rho_i))^2(\rho_{i+1} - \rho_i). \quad (22)$$

Such a scheme is the one used in [2].

2. **The Godunov/Godunov scheme:** a Godunov scheme for the convection term and a Godunov scheme for the diffusion term of the Taylor–expanded model Eq. (15):

$$f_i^{(2)} = G(\rho_i, \rho_{i+1}) + \frac{\tau}{dx} \rho_i V'(\rho_i) [G(\rho_{i+1}, \rho_{i+2}) - G(\rho_i, \rho_{i+1})]. \quad (23)$$

3. **The Godunov scheme:** a Godunov scheme for the modified convection term in the exact macroscopic model Eq. (14):

$$f_i^{(3)} = G \left(\frac{\rho_i}{1 - \frac{\tau}{dx}(V(\rho_{i+1}) - V(\rho_i))}, \frac{\rho_{i+1}}{1 - \frac{\tau}{dx}(V(\rho_{i+2}) - V(\rho_{i+1}))} \right). \quad (24)$$

Note that this scheme is valid if $1 - \frac{\tau}{dx}(V(\rho_{i+1}) - V(\rho_i)) > 0$ for all ρ_i and ρ_{i+1} . By denoting $V_0 = \sup_x V(x)$, this inequality holds if

$$\tau < dx/V_0. \quad (25)$$

Proposition 3.2 *The homogeneous configurations for which $\rho_i(t) = \rho_e$ for all i and t are linearly stable for the discrete traffic model Eq. 20 if and only if*

$$\alpha^2 + \beta^2 + \gamma^2 + \xi^2 - 2\alpha\gamma - 2\beta\xi + 2f(c_l) < 1, \quad \forall l = 1, \dots, N-1, \quad (26)$$

with $c_l = \cos(2\pi l/N)$ and $f(x) = (\alpha\beta + \alpha\xi + \beta\xi - 3\gamma\xi)x + 2(\alpha\gamma + \beta\xi)x^2 + 4\gamma\xi x^3$, and $\alpha = \frac{\partial F}{\partial \rho_i}$, $\beta = \frac{\partial F}{\partial \rho_{i+1}}$, $\gamma = \frac{\partial F}{\partial \rho_{i+2}}$ and $\xi = \frac{\partial F}{\partial \rho_{i-1}}$ the partial derivatives of the model in equilibrium.

Proof The perturbations to homogeneous solution are the variables $\varepsilon_i(t) = \rho_i(t) - \rho_e$. The perturbed system is

$$\begin{aligned} \varepsilon_i(t + dt) &= \rho_i(t + dt) - \rho_e = F(\rho_i(t), \rho_{i+1}(t), \rho_{i+2}(t), \rho_{i-1}(t)) - \rho_e \\ &= \alpha \varepsilon_i(t) + \beta \varepsilon_{i+1}(t) + \gamma \varepsilon_{i+2}(t) + \xi \varepsilon_{i-1}(t) + o(\text{LC}(\varepsilon_i, \varepsilon_{i-1}, \varepsilon_{i+1}, \varepsilon_{i+2})), \end{aligned} \quad (27)$$

with $\alpha = \frac{\partial F}{\partial \rho_i}$, $\beta = \frac{\partial F}{\partial \rho_{i+1}}$, $\gamma = \frac{\partial F}{\partial \rho_{i+2}}$ and $\xi = \frac{\partial F}{\partial \rho_{i-1}}$ at $(\rho_e, \rho_e, \rho_e, \rho_e)$. General conditions for the global stability of the discrete schemes can be obtained for a system of N cells with periodic boundary conditions. The linear perturbed system is $\vec{\varepsilon}(t+dt) = M \vec{\varepsilon}(t)$, with $\vec{\varepsilon} = {}^T(\varepsilon_1, \dots, \varepsilon_N)$ and M a sparse matrix with $(\xi, \alpha, \beta, \gamma)$ on the diagonal. If $M = PDP^{-1}$ with D a diagonal matrix, then $\vec{\varepsilon}(t) = PD^{t/dt}P^{-1}\vec{\varepsilon}(0) \rightarrow \vec{0}$ if all the coefficients of D are less than one excepted one equal to 1. M is circulant therefore the eigenvectors of M are $z(\iota^0, \iota^1, \dots, \iota^{m-1})$ with $\iota = \exp(i\frac{2\pi l}{N})$ and $z \in \mathbb{Z}$, and the eigenvalues are $\lambda_l = \alpha + \beta\iota_l + \gamma\iota_l^2 + \xi\iota_l^{-1}$. The system is linearly stable if $|\lambda_l| < 1$ for all $l = 1, \dots, N-1$. This is

$$\lambda_l^2 = \alpha^2 + \beta^2 + \gamma^2 + \xi^2 - 2\alpha\gamma - 2\beta\xi + 2f(c_l) < 1, \quad \forall l = 1, \dots, N-1, \quad (28)$$

with $c_l = \cos(2\pi l/N)$ and $f(x) = (\alpha\beta + \alpha\xi + \beta\xi - 3\gamma\xi)x + 2(\alpha\gamma + \beta\xi)x^2 + 4\gamma\xi x^3$. \blacksquare

These conditions Eq. (26) are applied to the different numerical schemes Eq. (22), Eq. (23) and Eq. (24) with optimal speed $V(\rho) = \frac{1}{T}(1/\rho - \ell)$, $T > 0$ being the vehicles time gap and $\ell \geq 0$ the vehicle' size. For such speed function, the Godunov scheme is simply $G(x, y) = \frac{1}{T}(1 - y\ell)$. \square

Lemma 3.3 *The homogeneous configurations are linearly stable for the Godunov-Euler scheme Eqs. (20-22) if*

$$2\tau < T\ell \, dx \, \rho_e^2, \quad (29)$$

and if dt is sufficiently small.

Proof Mixed with the scheme for the density Eq. (20), Godunov/Euler scheme Eq. (22) is

$$F_1(\rho_i, \rho_{i+1}, \rho_{i+2}, \rho_{i-1}) = \rho_i + \frac{dt}{T \, dx} \left(\ell(\rho_{i+1} - \rho_i) + \frac{\tau}{T \, dx} \left(\frac{\rho_i - \rho_{i-1}}{\rho_{i-1}^2} - \frac{\rho_{i+1} - \rho_i}{\rho_i^2} \right) \right), \quad (30)$$

where $\alpha = 1 - A + 2B$, $\beta = A - B$, $\gamma = 0$ and $\xi = -B$ with $A = \frac{dt \, \ell}{T \, dx}$ and $B = \frac{dt \, \tau}{(T \, dx \, \rho_e)^2}$.

If $\tau < \frac{1}{2}T\ell \, dx \, \rho_e^2$, then $\alpha > 0$ for

$$dt < \frac{T \, dx}{\ell + \frac{2\tau}{T \, dx \, \rho_e^2}}, \quad (31)$$

and for all $dt \geq 0$ if $\tau \geq \frac{1}{2}T\ell \, dx \, \rho_e^2$. Moreover $1 - \alpha > 0$ if $\tau < \frac{1}{2}T\ell \, dx \, \rho_e^2$ while β is positive only if $\tau < T\ell \, dx \, \rho_e^2$ and the sign of ξ is the one of $-\tau$.

The stability conditions are distinguished according to the sign of τ .

- If $\tau < 0$ and Eq. (31) holds, then $f(x) = \alpha(1 - \alpha)x + 2\beta\xi x^2$ is strictly convex and is maximal on $[-1, 1]$ for $x = -1$ or $x = 1$. Therefore the model is stable if $f(-1) < f(1)$; this is simply $-\alpha(1 - \alpha) < \alpha(1 - \alpha)$ that is always true since $\alpha > 0$ if (31) holds and $1 - \alpha > 0$ on $\tau < 0$. Therefore the system is stable for all $\tau < 0$.
- Several cases have to be distinguished for $\tau > 0$. We assume in the following that Eq. (31) holds.

- For $0 < \tau < \frac{1}{2}T\ell \, dx \, \rho_e^2$, we have $\alpha, 1 - \alpha, \beta > 0$, $\xi < 0$ and $f(x) = \alpha(1 - \alpha)x + 2\beta\xi x^2$ is strictly concave and maximal for $x_0 = -\frac{\alpha(1-\alpha)}{4\beta\xi} > 0$. The model is stable if $x_0 > 1$, this is

$$dt < \frac{T \, dx}{\ell} - \frac{2\tau}{(\ell \rho_e)^2}. \quad (32)$$

This condition is more restrictive than Eq. (31).

- For $\frac{1}{2}T\ell \, dx \, \rho_e^2 < \tau < T\ell \, dx \, \rho_e^2$, we have $\alpha, \beta > 0$, $1 - \alpha, \xi < 0$ and $f(-1) > f(1)$ therefore the model is unstable. More precisely, f maximal for $x_0 < -1$, i.e. the unstable solution have shortest wavelength if

$$dt < \left(\tau - \frac{1}{2}T\ell \, dx \, \rho_e^2 \right) \left(\frac{2\tau}{T \, dx \, \rho_e} \right)^{-2}. \quad (33)$$

This condition is also more restrictive than Eq. (31).

- For $\tau > T\ell \, dx \, \rho_e^2$, we have $\alpha > 0$, $1 - \alpha, \beta, \xi < 0$ and the system is unstable for all dt with shortest wavelength since $f(\cdot)$ strictly convex and $f(-1) > f(1)$. ■

The stability conditions for the Godunov/Euler splitting scheme Eq. (22) are summarised in Fig. 3. The same conditions as the continuous macroscopic model are obtained for $dx \rightarrow 0$ and $dt \rightarrow 0$ such that $dt/dx \rightarrow 0$.

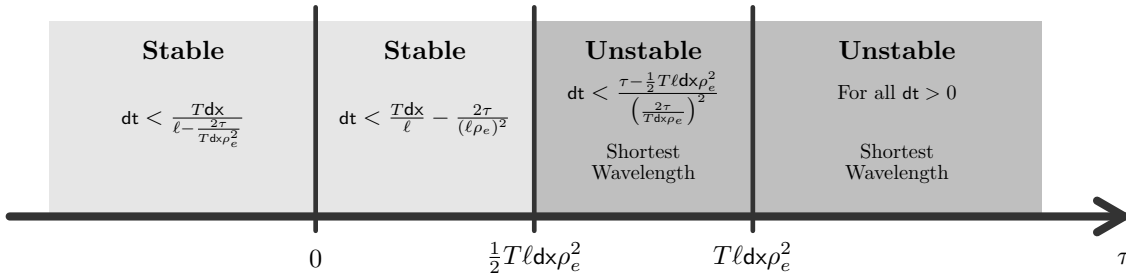


Figure 3: Summary of the stability conditions for the Godunov/Euler splitting scheme Eq. (22).

□

Lemma 3.4 *The homogeneous configurations are linearly stable for the Godunov-Euler schemes Eqs. (20-23) and Eqs. (20-24) if*

$$2|\tau| < T \, dx \, \rho_e, \quad (34)$$

and if dt is sufficiently small.

Proof The Godunov numerical schemes Eq. (23) and Eq. (24) are respectively

$$F_2(\rho_i, \rho_{i+1}, \rho_{i+2}, \rho_{i-1}) = \rho_i + \frac{dt \, \ell}{T \, dx} \left(\rho_{i+1} - \rho_i + \frac{\tau}{T \, dx} \left(\frac{\rho_{i+1} - \rho_{i+2}}{\rho_i} - \frac{\rho_i - \rho_{i+1}}{\rho_{i-1}} \right) \right), \quad (35)$$

and

$$F_3(\rho_i, \rho_{i+1}, \rho_{i+2}, \rho_{i-1}) = \rho_i + \frac{dt \, \ell}{T \, dx} \left(\frac{\rho_{i+1}}{1 - \frac{\tau}{T \, dx} \left(\frac{1}{\rho_{i+2}} - \frac{1}{\rho_{i+2}} \right)} - \frac{\rho_i}{1 - \frac{\tau}{T \, dx} \left(\frac{1}{\rho_{i+1}} - \frac{1}{\rho_i} \right)} \right). \quad (36)$$

By construction, both give $\alpha = 1 - A(1 + B)$, $\beta = A(1 + 2B)$, $\gamma = -AB$ and $\xi = 0$ with $A = \frac{dt \, \ell}{T \, dx}$ and $B = \frac{\tau}{T \, dx \, \rho_e}$. As expected, the stability conditions of these two schemes are the same.

If $\tau > -T \, dx \, \rho_e$, then $\alpha > 0$ for

$$dt < \frac{T \, dx}{\ell + \frac{\ell \tau}{T \, dx \, \rho_e}}, \quad (37)$$

and for all $dt \geq 0$ if $\tau \leq -T \, dx \, \rho_e$. β is positive only if $\tau > -\frac{1}{2}T \, dx \, \rho_e$. Moreover $1 - \beta > 0$ if Eq. (37) holds while the sign of γ is the one of $-\tau$.

Here again, the stability conditions are distinguished according to the sign of τ .

- If $\tau < 0$ and Eq. (37) holds, $f(x) = \beta(1 - \beta)x + 2\alpha\gamma x^2$ is strictly convex and is maximal on $[-1, 1]$ for $x = -1$ or $x = 1$. Therefore the model is stable if $f(-1) < f(1)$; this is

$$\tau > -\frac{1}{2}T \, dx \, \rho_e \quad \text{and} \quad dt < \frac{T \, dx}{\ell + \frac{2\ell\tau}{T \, dx \, \rho_e}}. \quad (38)$$

The condition for dt is weaker than (37) since τ is negative. If $\tau \leq -\frac{1}{2}T \, dx \, \rho_e$ then the system is unstable at the shortest wave-length frequency. A sufficient condition for that the finite system produces the shortest frequency is simply $N \geq 2$. Note that no condition holds on dt if $\tau \leq -T \, dx \, \rho_e$.

- If $\tau > 0$ and Eq. (37) holds then $f(x) = \beta(1 - \beta)x + 2\alpha\gamma x^2$ is concave and is maximum at $\arg \sup_x f(x) = x_0 = -\frac{\beta(1-\beta)}{4\alpha\gamma} > 0$. We know that $\lambda_0^2 = \alpha^2 + \beta^2 + \gamma^2 - 2\alpha\beta + f(1) = 1$ (case $l = 0$). Therefore the model is stable if $x_0 > 1$; this is

$$\tau < \frac{1}{2}T \, dx \, \rho_e \quad \text{and} \quad dt < \frac{T \, dx}{\ell} - \frac{2\tau}{\ell\rho_e}. \quad (39)$$

The condition for dt is stronger than Eq. (37). If $\tau \geq \frac{1}{2}T \, dx \, \rho_e$ then the system is unstable at the frequency $\cos^{-1}(x_0)$ that is reachable in the finite system if $N > 2\pi / \cos^{-1}(x_0)$. We have $x_0 \rightarrow 1/2 + T \, dx \, \rho_e / (4\tau)$ as $dt \rightarrow 0$, going from 1 to 1/2 according to τ (long wave). ■

The stability conditions for the Godunov/Godunov and Godunov schemes Eq. (23) and Eq. (24) are summarised in Fig. (4). The same conditions as the microscopic model are obtained at the limit $dt \rightarrow 0$ for $dx = 1/\rho_e$, i.e. a space step equal to the mean spacing.

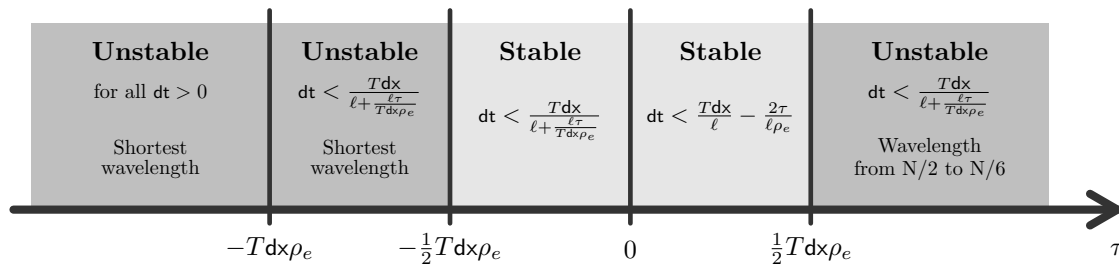


Figure 4: Summary of the stability conditions for the Godunov/Godunov and Godunov schemes Eq. (23) and Eq. (24). Note that we have the additional condition $\tau < dx/V_0$, with $V_0 = \sup_x V(x)$, for the simple Godunov scheme Eq. (24).

□

3.3 Bounds on the speed and the density

The microscopic model Eq. (5) is collision-free: the spacing remains by construction bigger than the vehicle length $\ell > 0$, and the speed is positive and bounded. We check whether this property also occurs with the numerical schemes F_j , $j = 1, 2, 3$ of the macroscopic models Eqs. (30), (35) and (36). The models are from the first order therefore the speed is necessary

positive and bounded if the optimal velocity functions are so defined. Moreover, the density remains bounded in $[1, \rho_M]$, with $\rho_M = 1/\ell$, if

$$F_j(0, a, b, c) \geq 0 \quad \text{and} \quad F_j(\rho_M, a, b, c) \leq \rho_M \quad \text{for all } (a, b, c). \quad (40)$$

It is easy to check that such property holds only if $\tau \leq 0$ for the Godunov/Euler Eq. (30), while it holds for $\tau \geq -dx\rho_e/W'$ with the Godunov/Godunov scheme Eq. (35), and for $\tau < dx/V_0$ with the simple Godunov scheme Eq. (36). As the microscopic model, Eq. (35) and Eq. (36) are able to describe macroscopically unstable homogeneous solutions with large waves by ensuring that speed and density remain positive and bounded. The relation between instability and self-sustained traffic waves (or jamiton) are notably described in [17, 34, 35, 41] with microscopic and macroscopic second order models. In the next section, we analyse by simulation the unstable solutions we get with the first order models for different initial conditions.

4 Simulation results

In this section numerical simulations of the microscopic model Eq. (5) and of the simple Godunov scheme Eq. (36) macroscopic model are compared. The car-following model Eq. (5) is simulated using an explicit Euler scheme. A ring (periodic boundaries) with a length 101 and 50 vehicles is considered. The optimal speed functions are $W(\Delta) = \max\{0, \min\{2, \Delta - 1\}\}$ and $V(\rho) = W(1/\rho)$ corresponding to a triangular fundamental diagram, while the reaction time is $\tau = 1$. The values of the parameters are set to obtain unstable homogeneous solutions. The time step is $dt = 0.01$. The space step for the Godunov scheme is the mean spacing $dx = 101/50 = 2.02$ in order to match the stability conditions of both microscopic and macroscopic model (see Eq. (6) and Fig. 4) and to hold the CFL conditions (see Eq. (25) and Fig. 4). Three experiments are carried out with different initial conditions. In the first one, the initial configuration is a jam. The initial condition is random in the second experiment while it is a perturbed homogeneous configuration in the last one.

4.1 Trajectories

In Figs. 5, 6 and 7, the trajectories of the microscopic model and the time series for the density by cell for the discrete macroscopic model (gray levels) are plot for respectively the jam, random and perturbed initial conditions. The jam stationary propagates within the first experiment in Fig. 5. Both microscopic and macroscopic models rigorously describe the same dynamics. The dynamics obtained does not perfectly coincide for the random and perturbed initial conditions (see Figs. 6 and 5). Yet most of the dynamics seems to be well recaptured and notably the self-sustained emergence of traffic stop-and-go waves. Note that the waves propagate backward with the speed $-\ell/T$ that is close to the value empirically observed (see [32]).

4.2 Fundamental diagram

The fundamental diagram is the plot of the flow or the mean speed as a function of the density. It generally refers to spatial performances [15], that have to be distinguished from temporal ones [45]. Here to deal with spatial performances, we measured the spatial speed and the density and express the flow as the product of the density by the speed. The density for the microscopic model is the inverse of the spacing (see Eq. (7)) while the speed in the macroscopic model is (see Eq. (9))

$$\tilde{V}(\rho_i, \rho_{i+1}) = V \left(\frac{\rho}{1 - \tau\rho(V(\rho_{i+1}) - V(\rho_i))} \right). \quad (41)$$

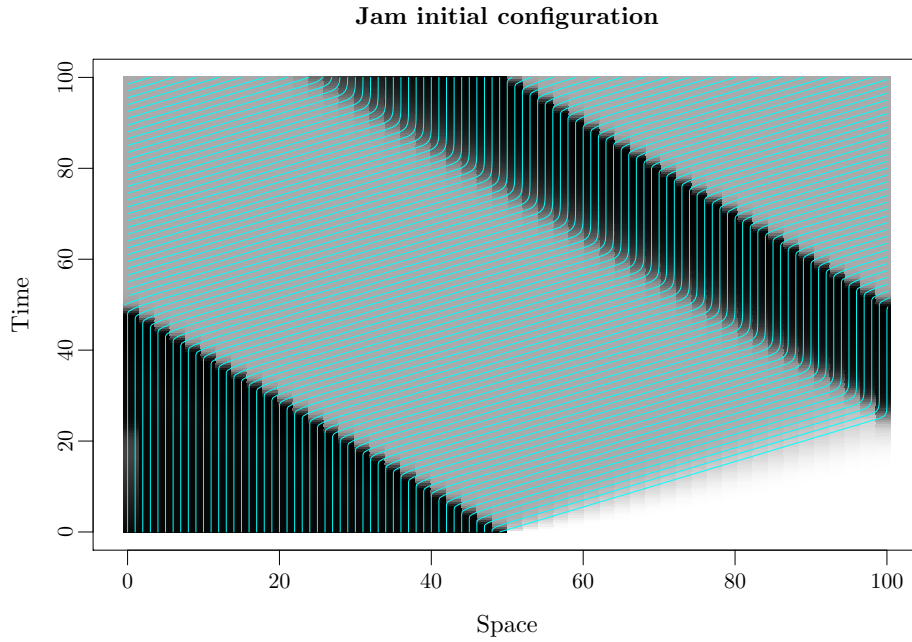


Figure 5: The trajectories of the microscopic model (cyan curves) and the time series for the density by cell for the discrete macroscopic model (gray levels) for jam initial conditions.

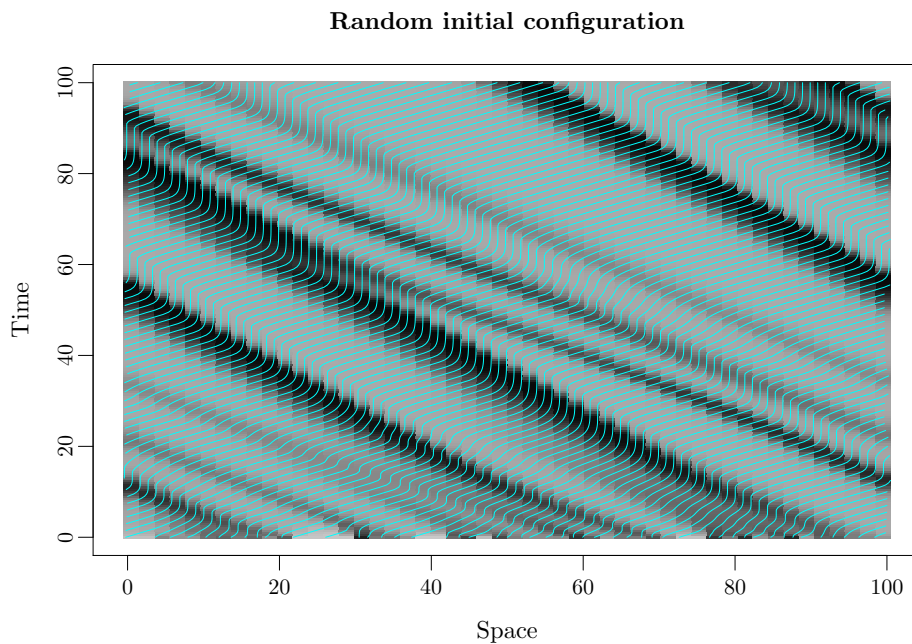


Figure 6: The trajectories of the microscopic model (cyan curves) and the time series for the density by cell for the discrete macroscopic model (gray levels) for random initial conditions.

The sequences obtained for the perturbed initial conditions (see Fig. 7) are presented in Fig. 8. The performances are *instantaneous* ones in the sense that they correspond to instantaneous

Perturbed initial configuration

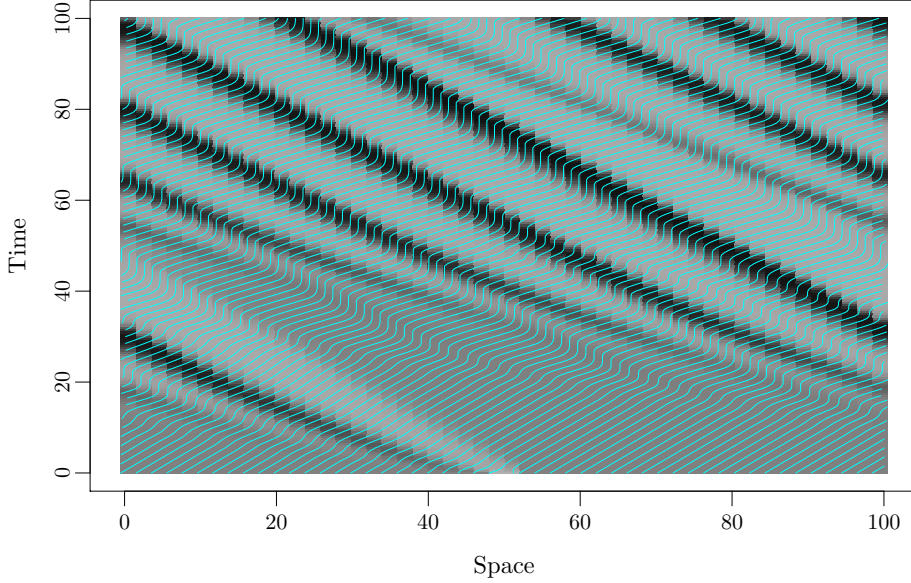


Figure 7: The trajectories of the microscopic model (cyan curves) and the time series for the density by cell for the discrete macroscopic model (gray levels) for perturbed initial conditions.

measurements for a vehicle (microscopic model) and a cell (macroscopic) in the system. The variability in such diagram is larger than the one of the *aggregated* fundamental diagram plotted in Fig. 1 where the performances were averaged over time intervals.

Both microscopic and macroscopic systems converge to limit-cycles with self-sustained stop-and-go waves resulting in hysteresis curves in the microscopic fundamental diagram. Such phenomenon generate scattering of the fundamental diagram for which some bounds can be calculated [47, 11, 19, 12, 41, 16]. The bounds V^+ and V^- for the fundamental diagrams can here intuitively be determined from the microscopic model. The upper bound V^+ corresponds to the sequence of a vehicle moving at maximal speed V_0 behind a stopped vehicle:

$$V^+(\rho) = \tilde{V}(\rho, 1/\ell) = V \left(\frac{\rho}{1 + \tau\rho V(\rho)} \right). \quad (42)$$

Due to the reaction time, the distance tends to be smaller and the fundamental diagram is ‘over-estimated’. Oppositely, the lower bound V^- corresponds to the sequence of a stopped vehicle following a predecessor moving at the maximal speed V_0 :

$$V^-(\rho) = \tilde{V}(\rho, 0) = V \left(\frac{\rho}{1 - \tau\rho(V_0 - V(\rho))} \right). \quad (43)$$

Here the reaction time induces a delay in the acceleration and an under-estimation of the fundamental diagram.

As in [41, 16], the bounds Eqs. (42) and (43) obtained with the macroscopic model are compared to real instantaneous pedestrians and road traffic data in Figs. 9 and 10. The pedestrians data comes from a laboratory experiment with participants in a ring geometry [18]. Several experiments have been carried out with different density levels. The road traffic data are real measurement of trajectories on an American highway [33]. The speed, density and the flow

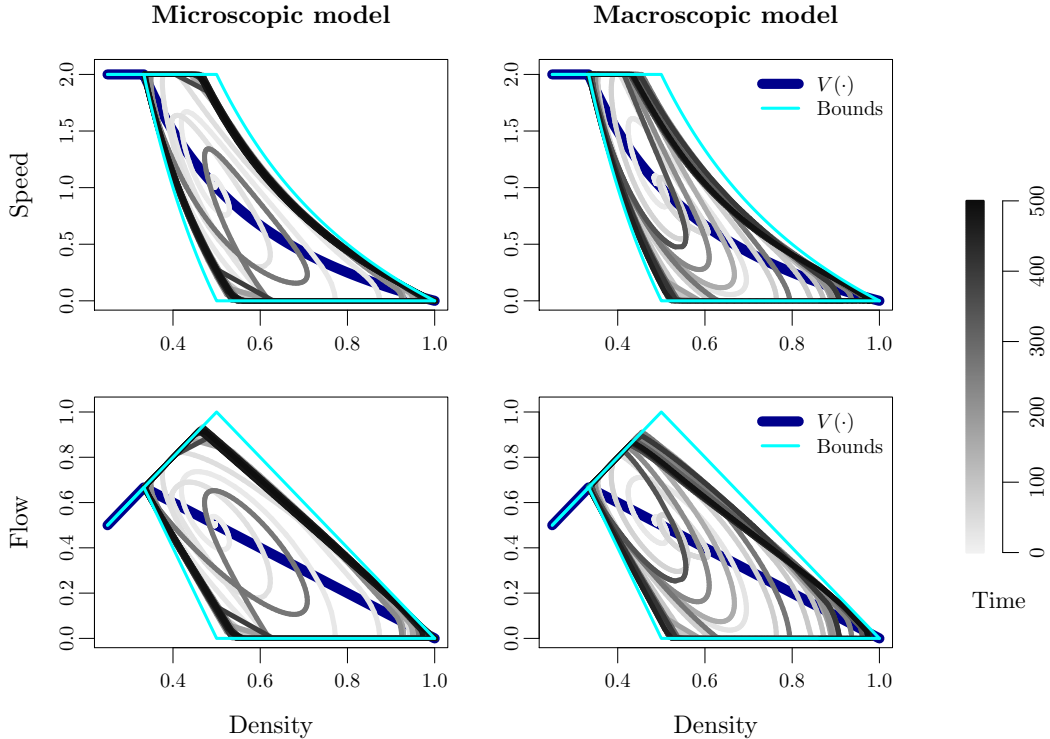


Figure 8: Sequence of speed and flow / density relation for the perturbed initial conditions (see Fig. 7). Left, for one vehicle (microscopic model) and right, for one cell (macroscopic model).

are measured as previously (i.e. the density is the inverse of the spacing while the flow is the product of the density by the speed). A triangular fundamental diagram with 3 parameters $V(\rho) = \min \left\{ V_0, \frac{1}{T}(1/\rho - 1) \right\}$ is used again. The parameters are the ones of an estimation by least squares for the pedestrians $V_0 = 0.9$ m/s, $\ell = 0.3$ m and $T = \tau = 1$ s, see Fig. 9, while $V_0 = 15$ m/s, $\ell = 5$ m and $T = \tau = 2$ s for the vehicles, see Fig. 10. The bounds present a reasonable agreement with the data, even if no clustering of measurements are observed around them.

5 Conclusion

Starting from a speed following model, we derive a first order convection-diffusion continuum traffic flow model that we discretised using Godunov and Euler schemes. Simulation results shown that discrete macroscopic models can recapture the dynamics of the microscopic model, if specific values for the space discretization are chosen. More precisely, the linear stability conditions of the homogeneous solutions for the macroscopic models match the ones of the microscopic model for specific values of the space discretization and sufficiently small time steps.

For unstable conditions, i.e. for large reaction times, the dynamics obtained describe self-sustained stop-and-go waves, with hysteresis cycles and a large scattering of the fundamental flow/density diagram. Such characteristics are observed in real data [44, 24, 23, 9, 48] as well as for second order models [47, 11, 19, 6, 17, 41, 12, 16]. Here it is achieved with first order

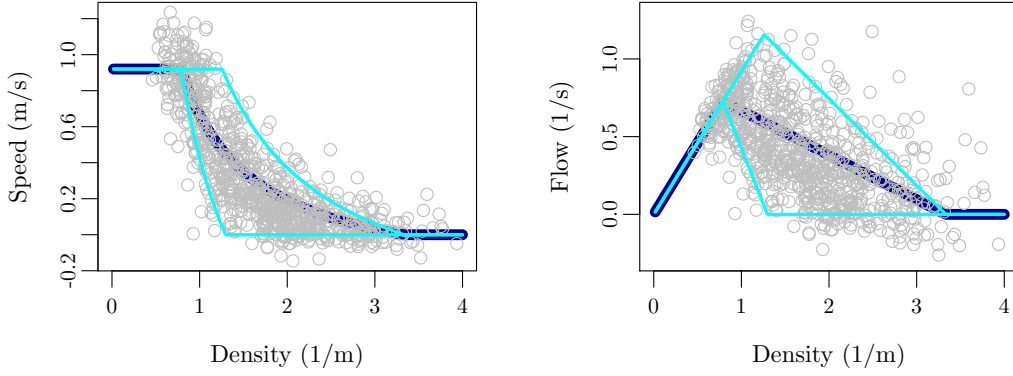


Figure 9: Instantaneous speed/density and flow/density measurements for real pedestrian flows [18] and the bounds Eqs. (42) and (43) for $V_0 = 0.9$ m/s, $\ell = 0.3$ m and $T = \tau = 1$ s.

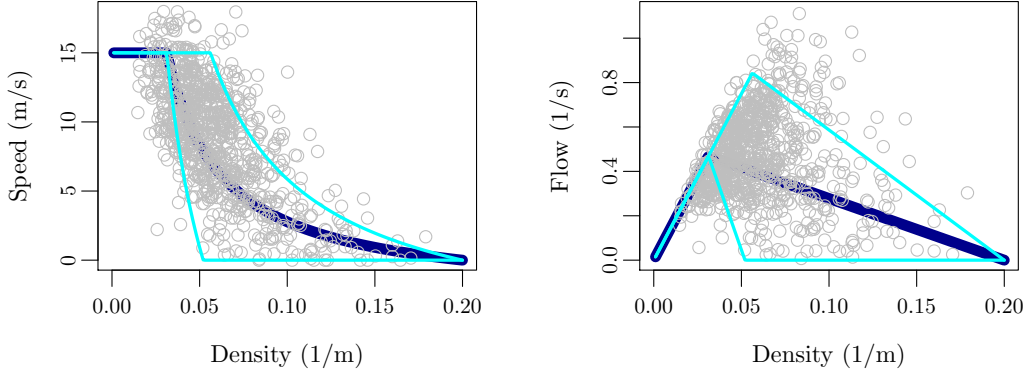


Figure 10: Individual speed/density and flow/density measurements for real road traffic flows [33] and the bounds Eqs. (42) and (43) for $V_0 = 15$ m/s, $\ell = 5$ m and $T = \tau = 2$ s.

models ensuring by construction that the models are physical and ‘collision-free’ (i.e. bounded and positive speed as well as density). Further investigations are necessary to understand the impact of the shape of the optimal velocity function on the characteristics of the waves. The macroscopic model corresponding to the follow-the-leader model is a first order elliptic convection-diffusion equation, for which the convection part is calibrated by the optimal velocity function (i.e. the fundamental diagram), while the diffusion is proportional to the reaction time parameter. More precisely the diffusion is negative in deceleration phases where the density get higher, and it is positive in acceleration phases where the density decreases. Such mechanism seems to be responsible for the appearance of oscillations and self-sustained non-linear stop-and-go waves in the system. This observation remains to be confirmed rigorously, yet it could give us a way to explain the wave formations.

References

- [1] C. Appert-Rolland, P. Degond, and S. Motsch. Two-way multi-lane traffic model for pedestrians in corridors. *Netw. Heterog. Media*, 6(3):351–381, 2011. [1](#)
- [2] A. Aw, A. Klar, M. Rascle, and T. Materne. Derivation of continuum traffic flow models from microscopic follow-the-leader models. *SIAM Journal on Applied Mathematics*, 63(1):259–278, 2002. [4](#), [7](#)
- [3] A. Aw and M. Rascle. Resurrection of "second order" models of traffic flow. *SIAM Journal on Applied Mathematics*, 60(3):916–938, 2000. [3](#)
- [4] M. Bando, K. Hasebe, A. Nakayama, A. Shibata, and Y. Sugiyama. Dynamical model of traffic congestion and numerical simulation. *Phys. Rev. E*, 51(2):1035–1042, 1995. [2](#), [3](#)
- [5] A. M. Bayen and C. G. Claudel. Lax–Hopf based incorporation of internal boundary conditions into Hamilton–Jacobi equation. Part I: Theory. *IEEE Transactions on automatic control*, 55(5):1142–1157, 2010. [1](#)
- [6] F. Berthelin, P. Degond, M. Delitala, and M. Rascle. A model for the formation and evolution of traffic jams. *Archive for Rational Mechanics and Analysis*, 187(2):185–220, 2008. [3](#), [14](#)
- [7] Sebastien Blandin, Dan Work, Paola Goatin, Benedetto Piccoli, and Alexandre Bayen. A general phase transition model for vehicular traffic. *SIAM journal on Applied Mathematics*, 71(1):107–127, 2011. [3](#)
- [8] R. Bürger and K. H. Karlsen. On a diffusively corrected kinematic-wave traffic flow model with changing road surface conditions. *Mathematical Models and Methods in Applied Sciences*, 13(12):1767–1799, 2003. [6](#)
- [9] D. Chowdhury, L. Santen, and A. Schadschneider. Statistical physics of vehicular traffic and some related systems. *Phys. Rep.*, 329(4-6):199–329, 2000. [2](#), [14](#)
- [10] M. Chraïbi, U. Kemloh, A. Schadschneider, and A. Seyfried. Force-based models of pedestrian dynamics. *Netw. Heterog. Media*, 6(3):425–442, 2011. [1](#)
- [11] R.M. Colombo. Hyperbolic phase transitions in traffic flow. *SIAM Journal on Applied Mathematics*, 63(2):708–721, 2003. [3](#), [13](#), [14](#)
- [12] R.M. Colombo, F. Marcellini, and M. Rascle. A 2-phase traffic model based on a speed bound. *SIAM Journal on Applied Mathematics*, 70(7/8):2652–2666, 2010. [3](#), [13](#), [14](#)
- [13] C. F. Daganzo. Requiem for second-order fluid approximations of traffic flow. *Transport. Res. B: Meth.*, 29(4):277–286, 1995. [2](#), [7](#)
- [14] L. C. Davis. Modifications of the optimal velocity traffic model to include delay due to driver reaction time. *Physica A*, 319(0):557–567, 2003. [2](#)
- [15] L.C. Edie. Discussion of traffic stream measurements and definitions. In J. Almond, editor, *Proc. of the 2nd International Symposium on Transportation and Traffic Theory*, pages 139–154, 1963. [11](#)
- [16] S. Fan, M. Herty, and B. Seibold. Comparative model accuracy of a data-fitted generalized Aw-Rascle-Zhang model. *Netw. Heterog. Media*, 9(2):239–268, 2014. [3](#), [13](#), [14](#)

- [17] M.R. Flynn, A.R. Kasimov, J.-C. Nave, R.R. Rosales, and B. Seibold. Self-sustained nonlinear waves in traffic flow. *Phys. Rev. E*, 79(5):056113, 2009. [3](#), [11](#), [14](#)
- [18] Forschungszentrum Jülich. Division Civil Safety and Traffic — <http://ped.fz-juelich.de/database>. [13](#), [15](#)
- [19] P. Goatin. The Aw–Rascle vehicular traffic flow model with phase transitions. *Mathematical and Computer Modelling*, 44(34):287–303, 2006. [3](#), [13](#), [14](#)
- [20] S. K. Godunov. A difference scheme for the numerical computation of a discontinuous solution of the hydrodynamic equation. *Math. Sbornik*, 47:271–306, 1959. [7](#)
- [21] J.M. Greenberg. Extensions and amplifications of a traffic model of Aw and Rascle. *SIAM Journal on Applied Mathematics*, 62(3):729–745, 2002. [3](#)
- [22] D. Helbing. *Verkehrsdynamik. Neue physikalische Modellierungskonzepte*. Springer Verlag, Berlin, Berlin, 1997. [1](#)
- [23] B. S. Kerner. Phase transitions in traffic flow. In D. Helbing, H. J. Herrmann, M. Schreckenberg, and D. E. Wolf, editors, *Traffic and Granular Flow '99*, pages 253–283, Berlin, Heidelberg, 2000. Springer Verlag. [2](#), [14](#)
- [24] B. S. Kerner and H. Rehborn. Experimental properties of phase transitions in traffic flow. *Phys. Rev. Lett.*, 79:4030–4033, 1997. [2](#), [14](#)
- [25] J.-P. Lebacque. Les modèles macroscopiques du trafic. *Annales des Ponts*, 67:24–45, 1993. [1](#)
- [26] J.-P. Lebacque. The Godunov scheme and what it means for first order traffic flow models. In J.-B. Lesort, editor, *Proc. of the 13th International Symposium on Transportation and Traffic Theory*, pages 647–677, 1996. [7](#)
- [27] J.-P. Lebacque, S. Mammari, and H. H. Salem. Generic second order traffic flow modelling. In *Proceedings of the 17th Symposium on Transportation and Traffic Theory*, pages 755–776. Elsevier, Oxford, 2007. [3](#)
- [28] Jean-Patrick Lebacque, H Haj-Salem, and Salim Mammari. Second order traffic flow modeling: supply-demand analysis of the inhomogeneous Riemann problem and of boundary conditions. In *Proceedings of the 10th Euro Working Group on Transportation (EWGT)*, 2005. [3](#)
- [29] M. H. Lighthill and G. B. Whitham. On kinematic waves II: a theory of traffic flow on long, crowded roads. In *Proceedings of the Royal Society of London series A*, volume 229, pages 317–345, 1955. [2](#)
- [30] P. Nelson. Synchronized traffic flow from a modified Lighthill–Whitman model. *Phys. Rev. E*, 61:R6052–R6055, 2000. [6](#)
- [31] G. F. Newell. Nonlinear effects in the dynamics of car-following. *Op. Res.*, 9(2):209–229, 1961. [2](#)
- [32] K. Nishinari, M. Treiber, and D. Helbing. Interpreting the wide scattering of synchronized traffic data by time gap statistics. *Phys. Rev. E*, 68:067101, 2003. [11](#)

- [33] US Department of Transportation. NGSIM: Next Generation Simulation — <http://www.ngsim.fhwa.dot.gov>. **13, 15**
- [34] G. Orosz and G. Stépán. Subcritical Hopf bifurcations in a car-following model with reaction-time delay. *Proc. Roy. Soc. London Ser. A*, 462(2073):2643–2670, 2006. **2, 11**
- [35] G. Orosz, R. E. Wilson, and G. Stépán. Traffic jams: dynamics and control. *Proc. Roy. Soc. London Ser. A*, 368(1928):4455–4479, 2010. **2, 11**
- [36] G. Orosz, R. E. Wilson, R. Szalai, and G. Stépán. Exciting traffic jams: Nonlinear phenomena behind traffic jam formation on highways. *Phys. Rev. E*, 80(4):046205, 2009. **2**
- [37] H. J. Payne. Models of freeway traffic and control. In *Mathematical Models of Public Systems, Simulation Council Proceedings Series*, volume 1, pages 51–61, 1971. **2**
- [38] L. A. Pipes. An operational analysis of traffic dynamics. *J. Appl. Phys.*, 24(3):274–281, 1953. **1**
- [39] P. I. Richards. Shock waves on a highway. *Op. Res.*, 4(1):42–51, 1956. **2**
- [40] A. Schadschneider and A. Seyfried. Empirical results for pedestrian dynamics and their implications for modeling. *Netw. Heterog. Media*, 6(3):545–560, 2011. **1**
- [41] B. Seibold, M.R. Flynn, A.R. Kasimov, and R.R. Rosales. Constructing set-valued fundamental diagrams from jamiton solutions in second order traffic models. *Netw. Heterog. Media*, 8(3):745–772, 2013. **3, 11, 13, 14**
- [42] A. Tordeux and A. Seyfried. Collision-free nonuniform dynamics within continuous optimal velocity models. *Phys. Rev. E*, 90:042812, 2014. **3**
- [43] M. Treiber and A. Kesting. *Traffic Flow Dynamics*. Springer, Berlin, 2013. **1, 2**
- [44] J. Treiterer and J.A. Myers. The hysteresis phenomenon in traffic flow. In D. J. Buckley, editor, *Transportation and Traffic Theory, Proceedings of the Sixth International Symposium*, pages 13–38, 1974. **2, 14**
- [45] J.H. Wardrop. Some theoretical aspects of road traffic research. *Proceedings of the Institution of Civil Engineers*, 1(3):325–362, 1952. **11**
- [46] G.B. Whitham. *Linear and Nonlinear Waves*. Pure and Applied Mathematics: A Wiley Series of Texts, Monographs and Tracts. Wiley, 2011. **2**
- [47] H.M. Zhang. A non-equilibrium traffic model devoid of gas-like behavior. *Transport. Res. B: Meth.*, 36(3):275–290, 2002. **3, 13, 14**
- [48] J. Zhang, W. Mehner, S. Holl, M. Boltjes, E. Andresen, A. Schadschneider, and A. Seyfried. Universal flow-density relation of single-file bicycle, pedestrian and car motion. *Physics Letters A*, 378(44):3274–3277, 2014. **2, 14**

Contents

1	Introduction	1
2	Microscopic and macroscopic models	3
2.1	The microscopic follow-the-leader model	3
2.2	Derivation of macroscopic models	3
3	Linear stability analysis	5
3.1	Linear stability analysis of the continuous macroscopic model	5
3.2	Linear stability analysis for the discrete schemes	6
3.3	Bounds on the speed and the density	10
4	Simulation results	11
4.1	Trajectories	11
4.2	Fundamental diagram	11
5	Conclusion	14
	References	16